Axisymmetric multiphase lattice Boltzmann method for generic equations of state

S.A. Reijers [a,*], H. Gelderblom [a], F. Toschi [b,c]

[a] Physics of Fluids Group, Faculty of Science and Technology, MESA+ Institute, University of Twente, P.O. Box 217, 7500 AE Enschede, The Netherlands
[b] Department of Applied Physics and Department of Mathematics and Computer Science, Eindhoven University of Technology, 5600 MB Eindhoven, The Netherlands
[c] IAC, CNR, Via dei Taurini 19, I-00185 Roma, Italy

ABSTRACT

We present an axisymmetric lattice Boltzmann model based on the Kupershtokh et al. multiphase model that is capable of solving liquid–gas density ratios up to 10^3. Appropriate source terms are added to the lattice Boltzmann evolution equation to fully recover the axisymmetric multiphase conservation equations. We validate the model by showing that a stationary droplet obeys the Young–Laplace law, comparing the second oscillation mode of a droplet with respect to an analytical solution and showing correct mass conservation of a propagating density wave.

© 2016 Elsevier B.V. All rights reserved.

1. Introduction

The lattice Boltzmann method (LBM) [1,2] is an efficient numerical tool to solve the Navier–Stokes equations. This numerical method can be systematically derived from the Boltzmann equations by means of a Hermite expansion approach [3]. In many physically realistic flow problems one has to deal with multiphase flows such as the contact angle hysteresis of a moving droplet on a surface, a capillary rise in a cylindrical tube and droplet impact on solid surfaces. To this end, several extensions have been proposed to support multiphase flows in the LBM. In an early attempt, Gunstensen et al. [4] studied a two-component fluid lattice-gas method. Shan et al. [5,6] were the first to incorporate intermolecular interactions to achieve phase separation in LBM. A different approach to model a multiphase fluid was developed by Swift et al. [7], who associated a free energy functional to the fluid. In their original form, these models lack the ability to achieve high density ratios across fluid interfaces and suffer from spurious currents near the liquid–vapor interface. In many engineering applications density ratios range from $10^1 to 10^3$, posing a serious limitation to the applicability of these lattice Boltzmann models in their original form. Recently, Lee et al. [8] showed that the spurious currents are caused by discretization errors in the computation of the multiphase force. These spurious currents can be reduced to machine

precision by employing a potential form of the non-ideal pressure and a isotropic central difference approximation scheme for the multiphase force. Kupershtokh et al. [9] showed that it is possible to achieve density ratios of 10^6 when the multiphase force is discretized by just a single-neighbour discretization scheme. The ability to achieve high density ratios makes this model applicable to many engineering applications. However, in this scheme the surface tension cannot be varied independently and spurious currents still exist.

Recently the LBM was extended to support axisymmetric multiphase flows. These axisymmetric simulations are effectively 2D simulations in a cylindrical coordinate system. Therefore, the computational cost for axisymmetric 3D flow problems is significantly lower in comparison to the same problem in a full 3D simulation. Halliday et al. [10] was the first to implement an axisymmetric LBM for single-phase flows. They introduced additional source and sink terms to the evolution equation and showed that they recover the 2D axisymmetric Navier–Stokes equations. This model was improved by Lee et al. [11] who corrected a missing source term related to the radial velocity. In addition, the method of Halliday et al. was extended to support non-ideal flows. Premnath et al. [12] were the first to implement an axisymmetric multiphase LBM. Their model is able to achieve density ratios up to 10 and was further improved by Mukherjee et al. [13] to support density ratios up to 10^3 and perform stable computations at lower viscosities. In this improved model, they use a pressure-evolution based LBM combined with a multiple-relaxation-time (MRT) collision model. Another axisymmetric multiphase LBM model by Srivastava et al.

* Corresponding author.
E-mail address: s.a.reijers@utwente.nl (S.A. Reijers).

[14] is based upon the widely used Shan–Chen model. In this model, they add an extra contribution to the Shan–Chen multiphase force to fully recover three-dimensionality in the system. However, large density ratios (>30) could not be achieved due to the limits of the original Shan–Chen model.

In this paper, we introduce a novel and easy-to-implement axisymmetric isothermal multiphase model for high density ratio fluids. The proposed model is based on the axisymmetric LBM of Srivastava et al. [14] combined with the multiphase model of Kupershtokh et al. [9]. The combined model inherits all advantages and disadvantages of the existing multiphase model by Kupershtokh et al., which we will not discuss in detail here. An extensive study to the accuracy and stability of the Kupershtokh et al. multiphase method can be found in [15]. Our implementation is discussed in Section 2. In Section 3 we present three validation tests. First, we verify that a stationary droplet obeys the Young–Laplace law. Then, we compare the second oscillation mode of an oscillating droplet with an incompressible analytical solution. Finally, we show that the method correctly describes the propagation of a density wave towards and away from the longitudinal z-axis. Our main conclusions and limitations of the method are discussed in Section 4.

2. Model derivation

We first introduce the standard LBM. In the following subsections, we will gradually show the changes necessary to obtain a fully functional axisymmetric isothermal multiphase LBM.

2.1. The lattice Boltzmann method

We use the common D2Q9 LBM, based on a two-dimensional Eulerian lattice with nine velocities. For the time evolution of the distribution function f_i, we use the BGK approximation with a single relaxation parameter τ [2]. The time evolution is given by

$$f_i(\boldsymbol{x}+\boldsymbol{e}_i\delta t, t+\delta t) = f_i(\boldsymbol{x}, t) + \frac{\delta t}{\tau}(f_i^{\text{eq}}(\boldsymbol{x}, t) - f_i(\boldsymbol{x}, t)) + \delta t S_i(\boldsymbol{x}, t), \quad (1)$$

where $\boldsymbol{x}$ is the position, t is the time, δt is the time step, τ is the relaxation time, $S_i(\boldsymbol{x}, t)$ is a source term, f_i^{eq} is the local equilibrium distribution and $\boldsymbol{e}_i$ is a discrete velocity set given by

$$\boldsymbol{e}_i = \begin{cases} (0, 0) & i = 0, \\ (1, 0)_{\text{FS}} & i = (1, 2, 3, 4), \\ (\pm 1, \pm 1) & i = (5, 6, 7, 8), \end{cases}$$

where the subscript $_{\text{FS}}$ denotes a fully symmetric set of points. The local equilibrium distribution function f_i^{eq} is a second-order Taylor expansion of the Maxwell–Boltzmann distribution [2] and is given by

$$f_i^{\text{eq}}(\boldsymbol{x}, t) = w_i\rho(\boldsymbol{x}, t)\left[1 + \frac{1}{c_s^2}(\boldsymbol{e}_i \cdot \boldsymbol{u}(\boldsymbol{x}, t)) + \frac{1}{2c_s^2}\right.$$
$$\left. \times \left(\frac{1}{c_s^2}(\boldsymbol{e}_i \cdot \boldsymbol{u}(\boldsymbol{x}, t))^2 - \|\boldsymbol{u}(\boldsymbol{x}, t)\|^2\right)\right], \quad (2)$$

where $c_s^2 = 1/3$ is the lattice speed of sound in this single-phase model and w_i are the quadrature weights given by

$$w_i = \begin{cases} 4/9 & i = 0, \\ 1/9 & i = (1, 2, 3, 4), \\ 1/36 & i = (5, 6, 7, 8). \end{cases}$$

The hydrodynamic quantities of the fluid, such as density ρ and velocity $\boldsymbol{u}$ are calculated as weighted sums of the distribution function f_i

$$\rho(\boldsymbol{x}, t) = \sum_i f_i(\boldsymbol{x}, t), \quad (3)$$

$$\boldsymbol{u}(\boldsymbol{x}, t) = \frac{\delta t \boldsymbol{F}(\boldsymbol{x}, t)}{2\rho(\boldsymbol{x}, t)} + \sum_i \frac{\boldsymbol{e}_i f_i(\boldsymbol{x}, t)}{\rho(\boldsymbol{x}, t)}, \quad (4)$$

where $\boldsymbol{u}(\boldsymbol{x}, t)$ is shifted by means of an internal/external force $\boldsymbol{F}$. In the past, different implementations of a body force, $\boldsymbol{F}$, were proposed [16]. Here we use the forcing scheme by Guo et al. [17]

$$S_i(\boldsymbol{x}, t) = w_i\left(1 - \frac{\delta t}{2\tau}\right)\left(\frac{(\boldsymbol{e}_i - \boldsymbol{u}) \cdot \boldsymbol{F}}{c_s^2} + \frac{(\boldsymbol{e}_i \cdot \boldsymbol{u})(\boldsymbol{e}_i \cdot \boldsymbol{F})}{c_s^4}\right). \quad (5)$$

2.2. The extension to an axisymmetric method

In an axisymmetric flow (Fig. 1), there is no flow in the azimuthal direction ($u_\theta = 0$) and mass conservation reads

$$\frac{\partial\rho}{\partial t} + \nabla_{\text{c}} \cdot (\rho\boldsymbol{u}) = -\frac{\rho u_r}{r} \quad (6)$$

where $\nabla_{\text{c}} \equiv (\partial/\partial z, \partial/\partial r)$ is the gradient operator in a two-dimensional Cartesian coordinate system ($x \to z, y \to r$) and $\boldsymbol{u} = (u_z, u_r)$ is the fluid velocity. The momentum equation reads

$$\rho\left(\frac{\partial\boldsymbol{u}}{\partial t} + \boldsymbol{u} \cdot \nabla_{\text{c}}\boldsymbol{u}\right) = -\nabla_{\text{c}}P + \mu\nabla_{\text{c}} \cdot [\nabla_{\text{c}}\boldsymbol{u} + \nabla_{\text{c}}\boldsymbol{u}^{\text{T}}] + \boldsymbol{C} \quad (7)$$

where P is the fluid pressure which in a single-phase LBM is given by $P = c_s^2\rho$ and $\boldsymbol{C}$ is given by

$$C_z = \frac{\mu}{r}\left(\frac{\partial u_z}{\partial r} + \frac{\partial u_r}{\partial z}\right), \quad C_r = 2\mu\frac{\partial}{\partial r}\left(\frac{u_r}{r}\right), \quad (8)$$

with μ the fluid viscosity. It is clear that Eqs. (6) and (7) have additional contributions to the mass and momentum conservation equations in comparison to 2D flow in the (z, r)-plane. These contributions ensure local conservation of mass and momentum when fluid is moving towards or away from the longitudinal z-axis. The single-phase LBM can be supplemented with appropriate source-terms to recover the axisymmetric conservation Eqs. (6) and (7) [14]. To this end, the evolution Eq. (1) is rewritten with an additional source term h_i

$$f_i(\boldsymbol{x} + \boldsymbol{e}_i\delta t, t + \delta t) = \frac{\delta t}{\tau}(f_i^{\text{eq}}(\boldsymbol{x}, t) - f_i(\boldsymbol{x}, t)) + f_i(\boldsymbol{x}, t) + \delta t S_i(\boldsymbol{x}, t)$$
$$+ \delta t h_i\left(\boldsymbol{x} + \boldsymbol{e}_i\frac{\delta t}{2}, t + \frac{\delta t}{2}\right). \quad (9)$$

where h_i is evaluated at fractional time steps. Srivastava et al. [14] showed by means of a Chapman–Enskog (CE) expansion that when h_i has the following form

$$h_i = w_i\left(-\frac{\rho u_r}{r} + \frac{1}{c_s^2}(e_{iz}H_z + e_{ir}H_r)\right), \quad (10)$$

with $\boldsymbol{e}_i = (e_{iz}, e_{ir})$ and

$$H_z = \frac{e_{iz}}{r}\left(\mu\left(\frac{\partial u_z}{\partial r} + \frac{\partial u_r}{\partial z}\right) - \rho u_r u_z\right), \quad (11\text{a})$$

$$H_r = \frac{e_{ir}}{r}\left(2\mu\left(\frac{\partial u_r}{\partial r} + \frac{u_r}{r}\right) - \rho u_r^2\right), \quad (11\text{b})$$

the resulting LBM solves the axisymmetric conservation equations given by (6) and (7) in the limit of small Mach number. The velocity derivatives inside (11) are approximated by a isotropic fifth-order

accurate finite difference scheme that will be given below (22). To have consistent boundary conditions, we use a symmetry boundary condition for the derivative evaluation at the axis and we impose a zero derivative for all other boundaries.

2.3. The extension to a multiphase axisymmetric method

We employ a temperature-dependent body force to obtain a multiphase fluid [5]. Zhang et al. [18] proposed a body force of the form

$$\boldsymbol{F}(\boldsymbol{x}, t) = -\nabla U(\boldsymbol{x}, t), \tag{12}$$

for which the overall effective fluid pressure in the system becomes

$$P(\boldsymbol{x}, t) = c_s^2 \rho(\boldsymbol{x}, t) + U(\boldsymbol{x}, t). \tag{13}$$

In this notation, it is evident that a particular equation of state (EOS) P_k can be obtained by simply adapting the choice for U accordingly

$$U(\boldsymbol{x}, t) = P_k(\boldsymbol{x}, t) - c_s^2 \rho(\boldsymbol{x}, t). \tag{14}$$

In this work, we will only consider the dimensionless van der Waals (vdW) EOS

$$P_k = \lambda \left(\frac{8\rho T}{3 - \rho} - 3\rho^2 \right), \tag{15}$$

$$c_k = \sqrt{\lambda \left(\frac{24T}{(\rho - 3)^2} - 6\rho \right)}, \tag{16}$$

where $T = T_{\mathrm{vdw}}/T_c$ is an effective temperature and T_c the critical temperature, c_k is the thermodynamic speed of sound at constant entropy, $\rho = \rho_{\mathrm{vdw}}/\rho_c$ is the density and ρ_c the critical density, $P = P_{\mathrm{vdw}}/P_c$ is the pressure and P_c the critical pressure and $\lambda = P_c/\rho_c(\frac{\delta t}{7}\Delta x)^2$ is a scaling parameter. Kupershtokh et al. [9] showed that for this vdW-EOS, the theoretical co-existence curve can be fully reconstructed by using the Exact-Difference-Method (EDM) forcing scheme and a special discretization for the body force

$$\boldsymbol{F}(\boldsymbol{x}) = \frac{18}{3\delta t} \left(A \sum_i w_i \psi^2(\boldsymbol{x} + \boldsymbol{e}_i \delta t) \boldsymbol{e}_i + (1 - 2A)\psi(\boldsymbol{x}) \sum_i w_i \psi(\boldsymbol{x} + \boldsymbol{e}_i \delta t) \boldsymbol{e}_i \right), \tag{17}$$

$$\psi(\boldsymbol{x}) = \sqrt{-P_k + \frac{\rho}{3}}. \tag{18}$$

where A is a tunable parameter. For $A = 0$ the scheme coincides with a local approximation scheme and for $A = 0.5$ with a mean-value approximation. The vdW co-existence curve is recovered by setting $A = -0.152$ [9].

By means of a Taylor expansion for $\psi(\boldsymbol{x} + \boldsymbol{e}_i \delta t)$ one can find a continuum expression for the body force

$$\boldsymbol{F}(\boldsymbol{x}) \approx \frac{18c_s^2}{3} \left(\psi(\boldsymbol{x})\nabla\psi(\boldsymbol{x}) + \frac{(\delta t)^2 c_s^2}{2} \right.$$

$$\left. \times \left[\psi(\boldsymbol{x})\nabla\nabla^2\psi(\boldsymbol{x}) + 6A\nabla\psi(\boldsymbol{x})\nabla^2\psi(\boldsymbol{x}) \right] \right) + \mathcal{O}((\delta t)^4) \tag{19}$$

To fully recover axisymmetry in the multiphase force, we need to use correction terms, similar to what has been done for the mass- and momentum conservation equations [14]. In cylindrical coordinates, the Laplace operator is given by $\nabla^2 \equiv \partial^2/\partial r^2 + \partial^2/\partial z^2 + (1/r)(\partial/\partial r) = \nabla_c^2 + (1/r)(\partial/\partial r)$. Therefore, we can rewrite (19) as

Table 1

Surface tension evaluated using (23). Here, A denotes the tuning parameter for the multi-phase force, while $\sigma_{\mathrm{lv}}^{2D}$ and $\sigma_{\mathrm{lv}}^{\mathrm{axis}}$ denote the surface tensions obtained from full (2D) and axisymmetric simulations. We find that the maximum relative error with 2D simulations is 1.3% for $A = 0$ and 3.2% for $A = -0.152$. An additional surface tension $\sigma_{\mathrm{lv}}^{\mathrm{lcs}}$ was simulated by using the lattice speed of sound c_s in (21). These results show an maximum relative error of 201% for $A = 0$ and 260% for $A = -0.152$. Simulation parameters: $N_z \times N_r = 500 \times 200$, $\tau = 1.5$, $\lambda = 0.01$.

T	$A = 0$			$A = -0.152$		
	$\sigma_{\mathrm{lv}}^{2D}$	$\sigma_{\mathrm{lv}}^{\mathrm{axis}}$	$\sigma_{\mathrm{lv}}^{\mathrm{lcs}}$	$\sigma_{\mathrm{lv}}^{2D}$	$\sigma_{\mathrm{lv}}^{\mathrm{axis}}$	$\sigma_{\mathrm{lv}}^{\mathrm{lcs}}$
0.9	0.305	0.304	0.606	0.371	0.383	0.965
0.8	0.928	0.928	1.865	1.146	1.158	2.884
0.7	1.983	2.009	3.909	2.285	2.318	5.681

$$\boldsymbol{F}(\boldsymbol{x}) \approx \frac{18c_s^2}{3} \left(\psi(\boldsymbol{x})\nabla_c\psi(\boldsymbol{x}) + \frac{(\delta t)^2 c_s^2}{2} \right.$$

$$\left. \times \left[\psi(\boldsymbol{x})\nabla_c\nabla_c^2\psi(\boldsymbol{x}) + 6A\nabla_c\psi(\boldsymbol{x})\nabla_c^2\psi(\boldsymbol{x}) \right] \right) +$$

$$\boldsymbol{F}_{\mathrm{axis}}(\boldsymbol{x}) + \mathcal{O}((\delta t)^4), \tag{20}$$

where $\boldsymbol{F}_{\mathrm{axis}}$ is given by

$$\boldsymbol{F}_{\mathrm{axis}}(\boldsymbol{x}) = 3(\delta t)^2 c_s^4 \left(\psi(\boldsymbol{x})\nabla_c \left[\frac{1}{r}\frac{\partial\psi(\boldsymbol{x})}{\partial r} \right] + \frac{6A}{r}\frac{\partial\psi(\boldsymbol{x})}{\partial r}\nabla_c\psi(\boldsymbol{x}) \right), \tag{21}$$

and can be identified as the cylindrical contribution to the multiphase force.

The meaning of c_s in the Taylor expansion that leads to (21) is ambiguous. When the lattice speed of sound (c_s) is used in (21), our validation tests for the surface tension showed a discrepancy in the range of 200–260% in comparison with full 2D simulations. By substituting the thermodynamic speed of sound c_k in (21) instead, we observe better consistency between the axisymmetric simulations and fully 2D simulations as is shown in Table 1 of the next section. Therefore, we use this substitution in the remainder of the paper. We attribute this ambiguity to the current mathematical formulation of the multiphase LBM. We use a lattice Boltzmann scheme that is derived from a single-phase ideal gas in which the speed of sound is assumed constant. However, by imposing a non-ideal EOS the speed of sound changes with density, which hence invalidates the constant lattice speed of sound. Unfortunately a mathematical proof of the validity of our substitution cannot be constructed at this moment and is left for future work.

The evaluation of $\boldsymbol{F}_{\mathrm{axis}}$ requires an approximation for the derivatives of ψ accurate up to order $(\delta t)^4$. Therefore, we use the following isotropic fifth-order accurate finite difference approximations given by (22) [14]. We use a symmetry boundary condition for the derivative evaluation at the axis and we impose a zero derivative for all other boundaries.
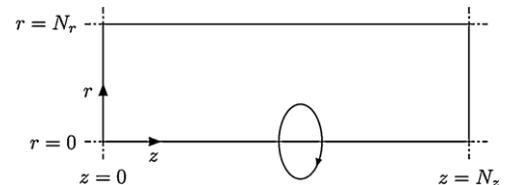

Fig. 1. Schematics of the axisymmetric geometry in our LBM. The Cartesian coordinates (x, y) are replaced with the axisymmetric coordinates (z, r). N_r is the length of the domain in the r-direction and N_z is the length in the z-direction.

$$\frac{\partial \psi(\boldsymbol{x})}{\partial r} = \frac{1}{36} \sum_{i=1}^{8} \left(8\psi(\boldsymbol{x} + \boldsymbol{e}_i \delta t) - \psi(\boldsymbol{x} + 2\boldsymbol{e}_i \delta t) \right) c_{ir} + \mathcal{O}((\delta t)^5),$$
(22a)

$$\frac{\partial^2 \psi(\boldsymbol{x})}{\partial r^2} = \frac{1}{36} \sum_{i=1}^{8} \left(\frac{8\partial\psi(\boldsymbol{x} + \boldsymbol{e}_i \delta t)}{\partial r} - \frac{\partial\psi(\boldsymbol{x} + 2\boldsymbol{e}_i \delta t)}{\partial r} \right) c_{ir}$$
$$+ \mathcal{O}((\delta t)^5),$$
(22b)

$$\frac{\partial \psi(\boldsymbol{x})}{\partial z} = \frac{1}{36} \sum_{i=1}^{8} \left(8\psi(\boldsymbol{x} + \boldsymbol{e}_i \delta t) - \psi(\boldsymbol{x} + 2\boldsymbol{e}_i \delta t) \right) c_{iz} + \mathcal{O}((\delta t)^5),$$
(22c)

$$\frac{\partial^2 \psi(\boldsymbol{x})}{\partial r \partial z} = \frac{1}{36} \sum_{i=1}^{8} \left(\frac{8\partial\psi(\boldsymbol{x} + \boldsymbol{e}_i \delta t)}{\partial z} - \frac{\partial\psi(\boldsymbol{x} + 2\boldsymbol{e}_i \delta t)}{\partial z} \right) c_{ir} + \mathcal{O}((\delta t)^5).$$
(22d)

3. Results and validation

Our model is capable of achieving density ratios up to 10^3. The co-existence curve relating the equilibrium vapor density ρ_v and liquid ρ_l density to the temperature T is plotted in Fig. 2. In the remainder of this section we validate our axisymmetric isothermal multiphase LBM against three test cases. First, we compare the pressure difference across the liquid–vapor interface of a stationary droplet of radius R_0 for different temperatures T to the Young–Laplace law. Then, we compare the second oscillation mode of an oscillating droplet with its analytical solution. Finally, we show that mass is correctly conserved by simulating a propagating density wave traveling towards and away from the longitudinal z-axis.

3.1. Stationary droplet validation

The pressure difference across the liquid–gas interface of a stationary 2D droplet with radius R_0 is given by the Young–Laplace equation

$$\Delta P_k = \frac{\sigma_{lv}}{R_0},$$
(23)

where $\sigma_{lv} = \sigma_{vdw}/(P_c \Delta x)$ is the surface tension between the liquid–vapor phase, $R_0 = R/\Delta x$ is the stationary droplet radius and $\Delta x = 1$ is the lattice spacing in our LBM. Note that there is only one radius of curvature in a two-dimensional system. In this validation test, we check if the value of the surface tension in the present model σ_{lv}^{axis} is consistent with a full 2D simulation σ_{lv}^{2D}. To this end, we perform simulations of a stationary droplet with radius $R_0 = 150$ (lattice units) for three different temperatures T and two coupling constants A. As boundary conditions for the axisymmetric simulation we use mid-grid specular reflection boundary condition on the longitudinal z-axis, periodic boundary conditions in the r direction and a free-slip boundary condition at $r = N_r$. In the 2D lattice Boltzmann simulation, we used periodic boundary conditions on all sides.

The results of these simulations are summarized in Table 1. When comparing the surface tension values between the full 2D and the axisymmetric simulation, we find that the maximum error
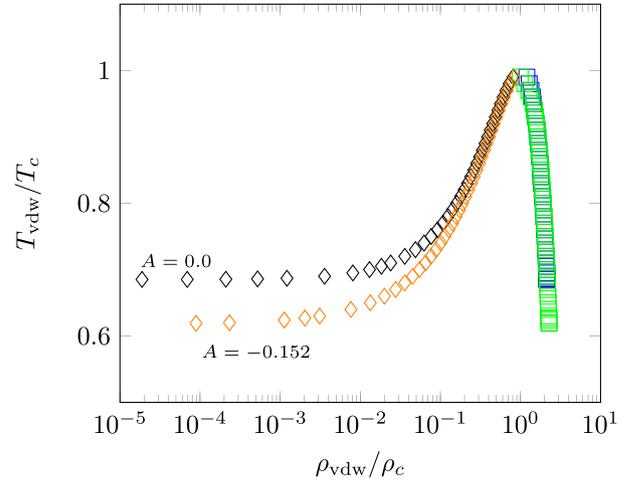

Fig. 2. The co-existence curve relating the equilibrium densities ρ_v and ρ_l to the temperature T for $A = 0$ (black diamonds and blue squares) and $A = -0.152$ (orange diamonds and green squares). The simulation is capable of achieving density ratios up to 10^3 and beyond. Simulation parameters: $N_z \times N_r = 150 \times 100$, $\tau = 1.0$, $\lambda = 0.01$. (For interpretation of the references to color in this figure legend, the reader is referred to the web version of the article.)

is 1.3% for $A = 0$ and 3.2% for $A = -0.152$, respectively. Our axisymmetric multiphase LBM is in excellent agreement with the full 2D counterpart.

3.2. Oscillating droplet validation

In this validation test we consider the problem of an oscillating axisymmetric droplet immersed in a gas. An analytical solution to the frequency and rate of damping of an oscillating droplet for arbitrary droplet radii, viscosity and surface tension was obtained by Miller and Scriven [19] in the limit of an isothermal, incompressible and Newtonian fluid. Here, we consider only the second mode which is axisymmetric

$$\omega_2 = \omega_2^* - \frac{\alpha(\omega_2^*)^{1/2}}{2} + \frac{\alpha^2}{4},$$
(24)

where

$$\omega_2^* = \sqrt{\frac{24\lambda\sigma_{lv}}{R_0^3(2\rho_v + 3\rho_l)}},$$
(25)

and

$$\alpha = \frac{25\sqrt{\nu_l\nu_v}\rho_l\rho_v}{\sqrt{2}R_0(2\rho_v + 3\rho_l)(\sqrt{\nu_l}\rho_l + \sqrt{\nu_v}\rho_v)},$$
(26)

with ν_v and ν_l the kinematic viscosities of the vapor and liquid phase, respectively.

In this test, we initialized the fluid domain with an axisymmetric ellipsoidal drop, $(r/R_a)^2 + (z/R_z)^2 = 1$, where R_a, R_b are the semi-principal lengths of the ellipsoid. The liquid and gas densities are initialized as the equilibrium densities to the corresponding temperatures. We measure the time dependent radius $R(t)$ of the droplet along the longitudinal z-axis for 4 different initial ellipsoid radii, see Figs. 3 and 4. Our simulation domain consists of a free-slip boundary condition at the top, periodic boundary conditions along the sides and the mid-grid specular reflection boundary condition on the longitudinal z-axis. The oscillation frequency ω_2 can be calculated by fitting the temporal evolution of the interfacial position with that of a damped harmonic oscillator $f(t) = a + b \exp(-ct) \sin(\omega_2 t + d)$, where the interfacial position is picked as the point in space where $\rho = (\rho_v + \rho_l/2)$. We found that the frequency ω_2 for the four different droplet radii have a minimal
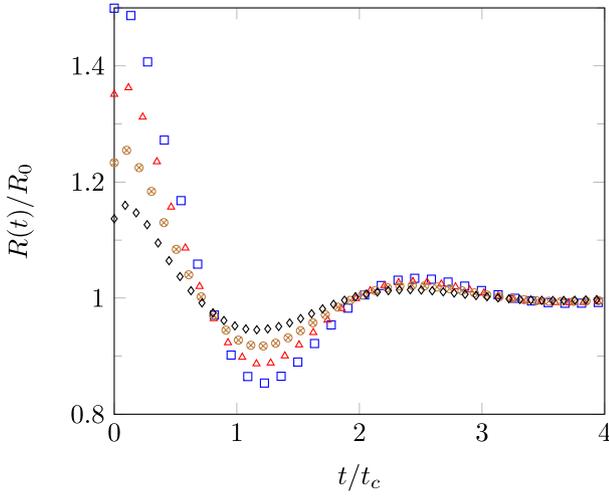
Fig. 3. The temporal evolution of the interfacial position along the longitudinal z-axis for four different initial conditions. We normalized the time by the capillary time $t_c = \sqrt{\rho R_0^3 / \lambda \sigma_{lv}}$ and the droplet radius R by its equilibrium radius R_0. Simulation parameters: $N_z \times N_r = 500 \times 250$, $\tau = 0.7$, $T = 0.8$, $A = 0.0$, $\lambda = 0.01$, $\rho_l / \rho_v \approx 10$.
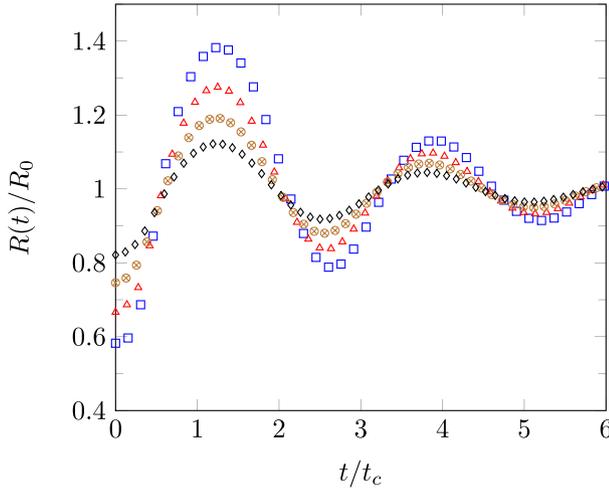

Fig. 4. The temporal evolution of the interfacial position along the longitudinal z-axis for four different initial conditions. We normalized the time by the capillary time $t_c = \sqrt{\rho R_0^3 / \lambda \sigma_{lv}}$ and the droplet radius R by its equilibrium radius R_0. Simulation parameters: $N_z \times N_r = 500 \times 250$, $\tau = 0.72$, $T = 0.655$, $A = -0.152$, $\lambda = 0.005$, $\rho_l / \rho_v \approx 130$.

relative error of 6% and a maximum relative error of 8% at density ratio $\rho_l / \rho_v \approx 10$ with respect to the incompressible analytical solution (24). For density ratio of $\rho_l / \rho_v \approx 130$, we found that the oscillation frequency ω_2 has a minimal relative error of 14.4% and a maximum relative error of 15.8%. Relative frequency errors ranging from 8% to 12% in oscillating droplets are also observed in other multiphase lattice Boltzmann models [13,20–23]. In order to show that this frequency error is not related to our axisymmetric implementation, we performed a full 2D oscillating droplet simulation at high density ratio. In this simulation, we used a square domain with 500 lattice units in each direction with periodic boundaries. We placed an ellipsoidal droplet with $R_0 = 150$ (lattice units) in the center of the domain with liquid and gas densities initialized as the equilibrium values to the corresponding temperature. The density ratio for this case was $\rho_l / \rho_v \approx 130$ with parameters $T = 0.655$, $\tau = 0.72$, $A = -0.152$ and $\lambda = 0.005$. The measured oscillation frequency ω_2 showed a relative error of 13.1% with respect to the analytical solution (24). We therefore conclude that the
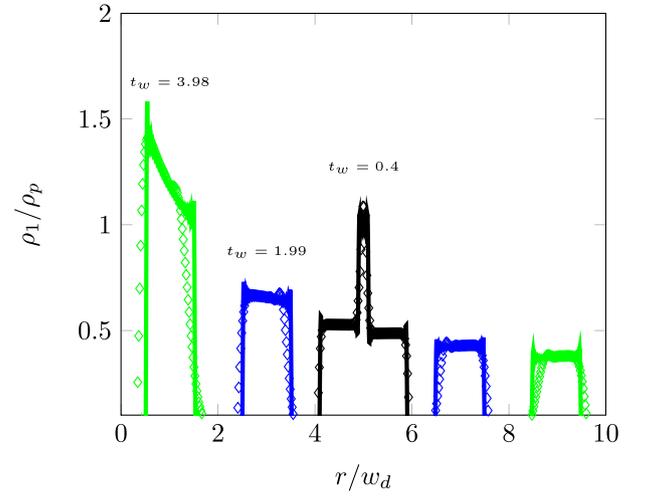

Fig. 5. The disturbance density field ρ_1 as function of the position r is plotted at different time stages, where $t_w = c_k t / w_d$ is the dimensionless time. Simulation parameters: $N_z \times N_r = 1 \times 2000$, $\tau = 0.6$, $T = 0.8$, $\rho = 1.8$, $A = 0.0$, $\lambda = 0.01$, $\rho_l / \rho_v \approx 10$.

discrepancy in the oscillation frequency is not related to our axisymmetric implementation. We also excluded that the discrepancy comes from finite size effects, therefore we suppose it may be due to a discrepancy between the physics modeled in our simulation and the idealized incompressible analytical solution (24).

3.3. Wave propagation validation

In the limit of small density fluctuations $\rho_1 / \rho_0 \ll 1$, the Navier–Stokes equations can be linearized up to first order, where ρ_1 is a density disturbance field and ρ_0 the background density [24]. The resulting cylindrical wave-equation for the disturbance field $\rho_1(\mathbf{x}, t)$ in the inviscid limit reads

$$\frac{\partial^2 \rho_1}{\partial t^2} - c_k^2 \nabla_c^2 \rho_1 = \frac{c_k^2}{r} \frac{\partial \rho_1}{\partial r}. \tag{27}$$

Here, we check if the mass of a propagating density wave towards and away from the axis is conserved and obeys the wave-equation (27). The spatial temporal solution for the cylindrical wave-equation (27) with an initial condition $\rho(r, 0)$ and a no-slip boundary condition at $r = R$, is given by [25]

$$\rho_1(r, t) = \frac{2}{R^2} \int_0^R \sum_{n=1}^{\infty} \rho_1(r', 0) \frac{J_0(k_n r / R) J_0(k_n r' / R)}{J_1(k_n)^2} \cos\left(\frac{c_k k_n}{R} t\right) r' dr', \tag{28}$$

where k_n is the nth zero of $J_0(k) = 0$, R is the channel height and $\rho_1(r', 0)$ is the initial condition.

We initialized the fluid domain with a uniform density ρ_0 supplemented with a small disturbance ρ_1 field of width w_d and amplitude ρ_p in the center of the domain at $t_w = 0$, where $t_w = c_k t / w_d$. In contrast to the oscillating droplet test, here we used the no-slip boundary condition at the top boundary, periodic boundary conditions along the sides and the mid-grid specular reflection boundary condition on the longitudinal z-axis. Furthermore, we set $\tau = 0.6$ to be in the limit of small viscosity. Fig. 5 shows the disturbance field ρ_1 as function of the position r at different time stages for both the simulation and analytic solutions (28). The initial density disturbance causes two propagating waves in the system: one wave traveling towards the longitudinal axis and one traveling away from the longitudinal axis. Fig. 5 clearly shows that mass is conserved in our simulation: there is a mass buildup in the wave traveling towards the longitudinal axis and mass loss for the wave traveling away from the longitudinal axis. We observe that the perturbed

density field in the simulation is in excellent agreement with the analytical solution. There is a small departure from the analytical solution at $t_w = 3.98$ as shown in Fig. 5. This departure is most likely caused by the dissipative nature of the LBM with $\tau = 0.6$, which is not described by (27).

4. Conclusion and discussion

We presented an axisymmetric LBM for high density ratio multiphase flows. The method is capable of achieving liquid-to-gas density ratios up to 10^3 and higher. In order to recover the axisymmetric multiphase mass and momentum conservation equations appropriate source terms are introduced in the lattice Boltzmann evolution equation and in the multiphase force. The source terms in the evolution equation ensure the correct modeling for the mass, momentum and viscous tensors, while the source terms in the multiphase force ensure a correct surface tension in the model.

In our axisymmetric formulation of the LBM we used correction terms for the multiphase force that scale with the lattice speed of sound. We substitute the thermodynamic speed of sound for the lattice speed of sound in this correction term. By doing so, we observe better consistency with the fully 2D counterpart. A mathematical proof of the validity of this substitution cannot be provided at this moment and is left for future work.

We validated the model by comparing the Young–Laplace pressure of the axisymmetric simulation with the full 2D simulations. We observe a maximum relative error in the Laplace pressure of 3.2%. Then, we validated the dynamics of an axially symmetric oscillating droplet with a known analytical solution. Here, we observe a maximum relative error of 15.8%. Finally, we validate that a propagating density wave moving towards and away from the longitudinal z-axis correctly conserves mass and found excellent agreement with the inviscid analytical solution.

References

[1] Z. Benzi, S. Succi, M. Vergassola, The lattice Boltzmann equation: theory and applications, Phys. Rep. 222 (1992) 145–197.
[2] Z. Guo, C. Shu, Lattice Boltzmann Method and its Applications in Engineering, 1st ed., World Scientific, Singapore, 2013.
[3] X. Shan, X. Yuan, H. Chen, Kinetic theory representation of hydrodynamics: a way beyond the Navier–Stokes equation, J. Fluid Mech. 550 (2006) 413–441.
[4] A. Gunstensen, D.H. Rothman, S. Zaleski, Z. Gianluigi, Lattice Boltzmann model of immiscible fluids, Phys. Rev. A 43 (1991) 4320–4327.
[5] X. Shan, H. Chen, Lattice Boltzmann model for simulating flows with multiple phases and components, Phys. Rev. E 47 (1993) 1815–1820.
[6] X. Shan, H. Chen, Simulation of nonideal gases and liquid–gas phase transitions by the lattice Boltzmann equation, Phys. Rev. E 49 (1994) 2941–2948.
[7] M. Swift, W. Osborn, J. Yeomans, Lattice Boltzmann simulation of nonideal fluids, Phys. Rev. Lett. 75 (1995) 830–834.
[8] T. Lee, P. Fischer, Eliminating parasitic currents in the lattice Boltzmann equation method for nonideal gases, Phys. Rev. E 74 (2006) 046709.
[9] A. Kupershtokh, D. Medvedev, D. Karpov, On equations of state in a lattice Boltzmann method, Comput. Math. Appl. 58 (2009) 965–974.
[10] I. Halliday, L. Hammond, C. Care, K. Good, A. Stevens, Lattice Boltzmann equation hydrodynamics, Phys. Rev. E 64 (2001) 011208.
[11] T. Lee, H. Huang, An axisymmetric incompressible lattice Boltzmann model for pipe flow, Int. J. Mod. Phys. C 17 (2006) 645–661.
[12] K. Premnath, J. Abraham, Lattice Boltzmann model for axisymmetric multiphase flows, Phys. Rev. E 71 (2005) 056706.
[13] S. Mukherjee, J. Abraham, Lattice Boltzmann simulations of two-phase flow with high density ratio in axially symmetric geometry, Phys. Rev. E 75 (2007) 026701.
[14] S. Srivastava, P. Perlekar, J. Thije Boonkkamp, N. Verma, F. Toschi, Axisymmetric multiphase lattice Boltzmann method, Phys. Rev. E 88 (2013) 013309.
[15] A. Hu, L. Li, R. Uddin, Force method in a pseudo-potential lattice Boltzmann model, J. Comput. Phys. 294 (August) (2015) 78–89.
[16] H. Huang, M. Krafczyk, X. Lu, Forcing term in single-phase and Shan–Chen-type multiphase lattice Boltzmann models, Phys. Rev. E 84 (2011) 046710.
[17] Z. Guo, C. Zheng, S. Baochang, Discrete lattice effects on the forcing term in the lattice Boltzmann method, Phys. Rev. E 65 (2002) 046308.
[18] R. Zhang, H. Chen, Lattice Boltzmann method for simulations of liquid–vapor thermal flows, Phys. Rev. E 67 (2003) 066711.
[19] C. Miller, L. Scriven, The oscillations of a fluid droplet immersed in another fluid, J. Fluid Mech. 32 (1968) 417–435.
[20] H. Huang, M. Sukop, X. Lu, Multiphase Lattice Boltzmann Methods: Theory and Application, 1st ed., Wiley-Blackwell, 2015, pp. 219–222.
[21] K.N. Premnath, J. Abraham, Three-dimensional multi-relaxation time (MRT) Lattice-Boltzmann models for multiphase flow, J. Comput. Phys. 224 (2007) 539–559.
[22] A. Xu, T. Zhao, L. An, L. Shi, A three-dimensional pseudo-potential-based lattice Boltzmann model for multiphase flows with large density ratio and variable surface tension, Int. J. Heat Fluid Flow 56 (2015) 261–271.
[23] K. Küllmer, A. Krämer, D. Reith, W. Joppich, H. Foysi, Numerical optimisation of the pseudopotential-based lattice Boltzmann method, J. Comput. Sci. (2016), http://dx.doi.org/10.1016/j.jocs.2016.04.005.
[24] E. Skudrzyk, The Foundations of Acoustics, 1st ed., Springer, Wien, 1971.
[25] D.G. Duffy, Green's Functions with Applications, 2nd ed., Taylor & Francis Group, 2015.

Sten Reijers is a PhD candidate in the Physics of Fluids group at the University of Twente, Netherlands. He obtained his masters degrees in Applied Physics from the University of Technology Eindhoven, Netherlands. His main research interests include droplet dynamics, fragmentation, high-density ratio multiphase flows and lattice Boltzmann methods.

Hanneke Gelderblom obtained her PhD degree in the Physics of Fluids group at the University of Twente. She is currently working as scientific project leader for the Dutch Foundation for Fundamental Research on Matter (FOM). Her research focusses on droplets, evaporation, impact, solidification and fragmentation.

Prof. Dr. Federico Toschi has advanced experience in fluid dynamics including numerical methods for turbulent, multiphase and thermal flows. His research activities focus on the statistical properties of fluids and in particular turbulence as well as in the modeling of flows at the nano- and micro-scales. He is currently chair of the COST Action MP1305 on "Flowing matter" and chair of a previous COST Action MP0806 on "Particles in turbulence". He is an editor for Journal of Turbulence, fellow of the American Physical Society (2015) and of the European Mechanics Society (2012).